

Stress-induced unfolded protein response contributes to Zika virus-associated microcephaly

Ivan Gladwyn-Ng¹, Lluís Cordón-Barris¹, Christian Alfano¹, Catherine Creppe¹, Thérèse Couderc^{2,3}, Giovanni Morelli^{1,4}, Nicolas Thelen¹, Michelle America¹, Bettina Bessières^{5,6}, Férechté Encha-Razavi⁵, Maryse Bonnière⁵, Ikuo K. Suzuki⁷, Marie Flamand⁸, Pierre Vanderhaeghen^{7,9}, Marc Thiry¹, Marc Lecuit^{1,2,3,10*} and Laurent Nguyen^{1*}

Accumulating evidence support a causal link between Zika virus (ZIKV) infection during gestation and congenital microcephaly. However, the mechanism of ZIKV-associated microcephaly remains unclear. We combined analyses of ZIKV-infected human fetuses, cultured human neural stem cells and mouse embryos to understand how ZIKV induces microcephaly. We show that ZIKV triggers endoplasmic reticulum stress and unfolded protein response in the cerebral cortex of infected postmortem human fetuses as well as in cultured human neural stem cells. After intracerebral and intraplacental inoculation of ZIKV in mouse embryos, we show that it triggers endoplasmic reticulum stress in embryonic brains in vivo. This perturbs a physiological unfolded protein response within cortical progenitors that controls neurogenesis. Thus, ZIKV-infected progenitors generate fewer projection neurons that eventually settle in the cerebral cortex, whereupon sustained endoplasmic reticulum stress leads to apoptosis. Furthermore, we demonstrate that administration of pharmacological inhibitors of unfolded protein response counteracts these pathophysiological mechanisms and prevents microcephaly in ZIKV-infected mouse embryos. Such defects are specific to ZIKV, as they are not observed upon intraplacental injection of other related flaviviruses in mice.

The cerebral cortex is an evolutionarily advanced brain structure made of neuronal layers tangentially organized into areas that serve higher cognitive functions. Its development commences from the formation and patterning of the neural tube, which progressively generates different classes of neurons that migrate and eventually settle into radially organized layers^{1,2}. These neurons are sequentially generated by distinct lineage-related progenitors. Upon the onset of corticogenesis, the first-born apical progenitors (APs) expand their number by symmetric division. These APs further undergo asymmetric division to give birth directly to neurons (direct neurogenesis) and later via the intermediary production of basal progenitors (indirect neurogenesis; Supplementary Fig. 1a; reviewed in ref. ³).

In humans, most malformations of cortical development affect cells that contribute to the formation of the cerebral cortex during the first two trimesters of pregnancy^{4,5}. Microcephaly is a common malformation of cortical development, clinically presenting in reductions in head circumference and brain size, due to improper generation and/or survival of neurons or their progenitors. Whilst congenital microcephaly is often caused by genetic defects, environmental factors and infectious agents transmitted vertically can also lead to this phenotype⁶. Recent observations of human fetuses^{7–9}, as well as experimental data obtained in animal models, strongly support the hypothesis that maternal–fetal transmission of ZIKV, a mosquito-borne virus of the Flaviviridae family, causes microcephaly^{10,11}. Furthermore, ZIKV impairs both the generation and

survival of neurons deriving from ZIKV-infected cortical progenitors^{12–16} and thus selectively interferes with developmental steps underlying cortex formation. However, the underlying molecular mechanisms of ZIKV-induced microcephaly in vivo remain poorly understood. Here we analyzed ZIKV-infected human cortical samples and mouse embryos to understand the pathophysiological mechanisms of ZIKV-induced microcephaly. We show that ZIKV triggers endoplasmic reticulum (ER) stress and an unfolded protein response (UPR) in the cerebral cortex of infected postmortem human fetuses as well as in cultured human neural stem cells. By using intracerebral or intraplacental injection of mouse embryos, we confirmed that ZIKV induces ER stress in vivo. This leads to microcephaly by deregulating a physiological UPR controlling the proper generation and survival of projection neurons during cerebral cortex development. Preventing UPR activation with pharmacological inhibitors upon ZIKV infection counteracts these pathophysiological mechanisms and prevents microcephaly in ZIKV-infected mouse embryos.

Results

ZIKV infection induces ER stress and activates UPR in human cortices and cultured neural stem cells. We have recently demonstrated that interfering with a physiological UPR in the cortical APs leads to congenital microcephaly by altering the balance between direct and indirect neurogenesis (Supplementary Fig. 1a)¹⁷. Since ZIKV has been reported to infect APs^{16,18} and replicate in

¹GIGA-Neurosciences, Interdisciplinary Cluster for Applied Genoproteomics (GIGA-R), University of Liège, C.H.U. Sart Tilman, Liège, Belgium. ²Institut Pasteur, Biology of Infection Unit, Paris, France. ³Inserm U1117, Paris, France. ⁴BIOMED - Hasselt University, Hasselt, Belgium. ⁵Département d'Histologie-Embryologie-Cytogénétique, Hôpital Necker-Enfant Malades, Paris, France. ⁶Inserm U 1163 Institut Imagine, Paris, France. ⁷Université Libre de Bruxelles (ULB), Institute for Interdisciplinary Research in Human Biology (IRIBHM), and ULB Institute of Neuroscience (UNI), Brussels, Belgium. ⁸Institut Pasteur, Structural Virology Unit, Paris, France. ⁹WELBIO, Université Libre de Bruxelles, Brussels, Belgium. ¹⁰Paris Descartes University, Sorbonne Paris Cité, Division of Infectious Diseases and Tropical Medicine, Necker-Enfants Malades University Hospital, Institut Imagine, Paris, France. Ivan Gladwyn-Ng, Lluís Cordon Barris, Christian Alfano, Catherine Creppe and Thérèse Couderc contributed equally to this work. *e-mail: marc.lecuit@pasteur.fr; lnguyen@ulg.ac.be

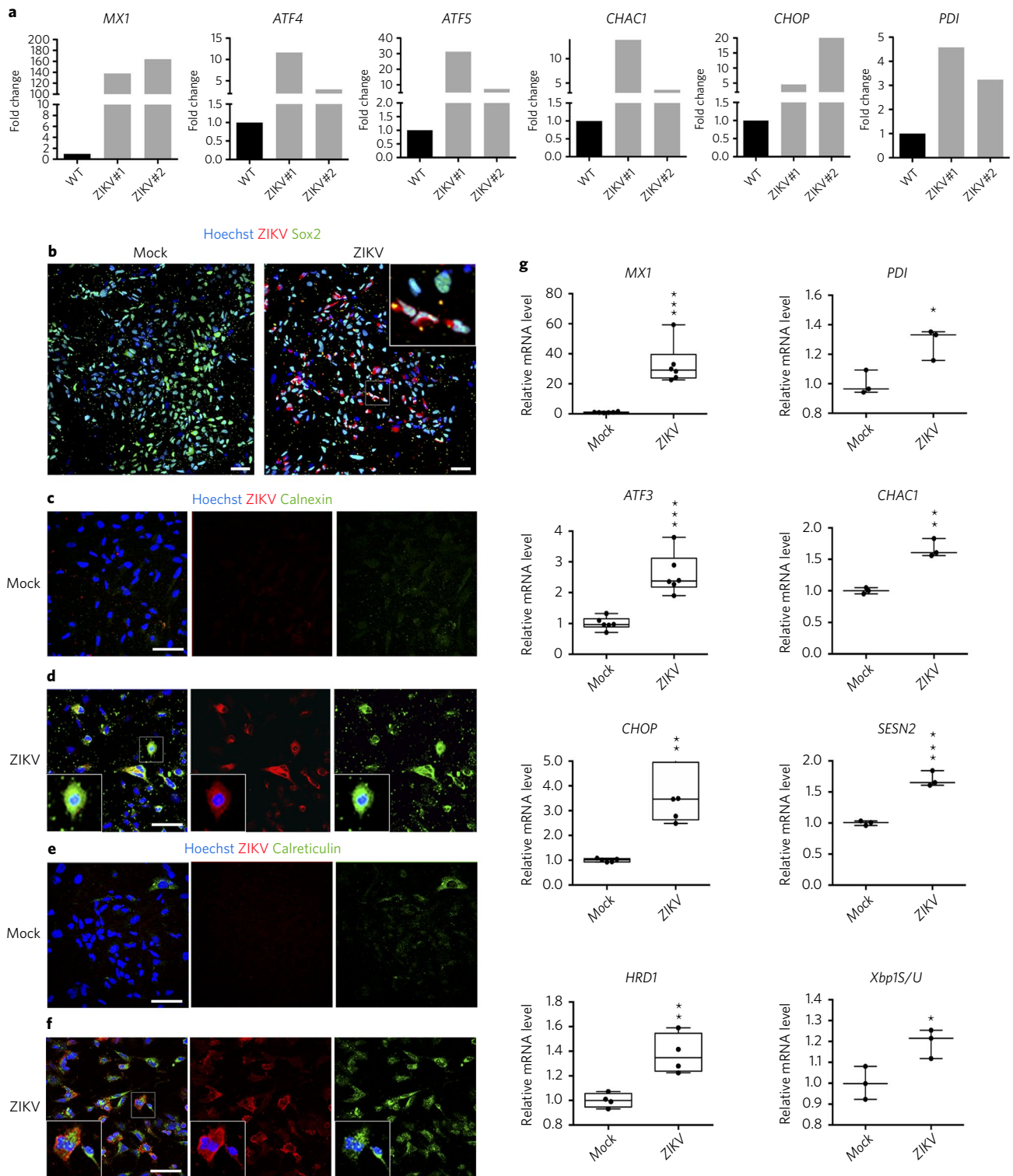


Fig. 1 | ZIKV induces ER stress and UPR in human cortices in vivo and in hNSCs in vitro. **a**, Histograms showing fold change of *MX1*, *ATF4*, *ATF5*, *CHAC1*, *CHOP* and *PDI* transcripts in occipital cortex from three control fetuses (WT; the value is normalized to 1 and corresponds to three WT at developmental ages of 21 GW, 23 GW and 24 GW) and two 22-GW fetuses infected by ZIKV during pregnancy (each histogram representing one fetus, ZIKV#1 and ZIKV#2 respectively; number of ZIKV copies per μg of extracted RNA = 1.39×10^4 for ZIKV#1, RNA = 3.32×10^6 for ZIKV#2, average number of ZIKV copies per μg of extracted RNA = $2.50 \times 10^6 \pm 1.27 \times 10^6$, mean \pm s.e.m.). **b-f**, Immunolabeling of mock- or ZIKV-infected hNSCs showing (**b**) Hoechst (blue), ZIKV (red) and Sox2 (green), (**c,d**) calnexin (green) or (**e,f**) calreticulin (green; $n = 5$ biologically independent replicates per condition). **g**, qRT-PCR performed on total RNA extract from mock- or ZIKV-infected hNSCs (average number of ZIKV copies per μg of extracted RNA = $1.10 \times 10^9 \pm 3.28 \times 10^8$, mean \pm s.e.m.) to detect *MX1* ($^{**}P = 0.0011$, $U = 0$), *PDI* ($^{*}P = 0.05$, $U = 0$), *ATF3* ($^{***}P < 0.001$, $U = 0$), *CHAC1* ($^{***}P = 0.0011$, $U = 0$), *CHOP* ($^{***}P = 0.0011$, $U = 0$), *SESN2* ($^{***}P < 0.001$, $U = 0$), *HRD1* ($^{**}P = 0.0011$, $U = 0$) and *XBP1S/U* ($^{*}P = 0.05$, $U = 0$). Data are analyzed by one-sided Mann-Whitney tests and presented as boxplots of median \pm first to third quartiles; whiskers extend to maxima and minima with each symbol representing $n = 3-6$ biologically independent samples, as indicated on respective boxplots. Scale bars represent 25 μm in **b** or 50 μm in **c-f**. $^{***}P < 0.001$, $^{**}P < 0.01$ and $^{*}P < 0.05$.

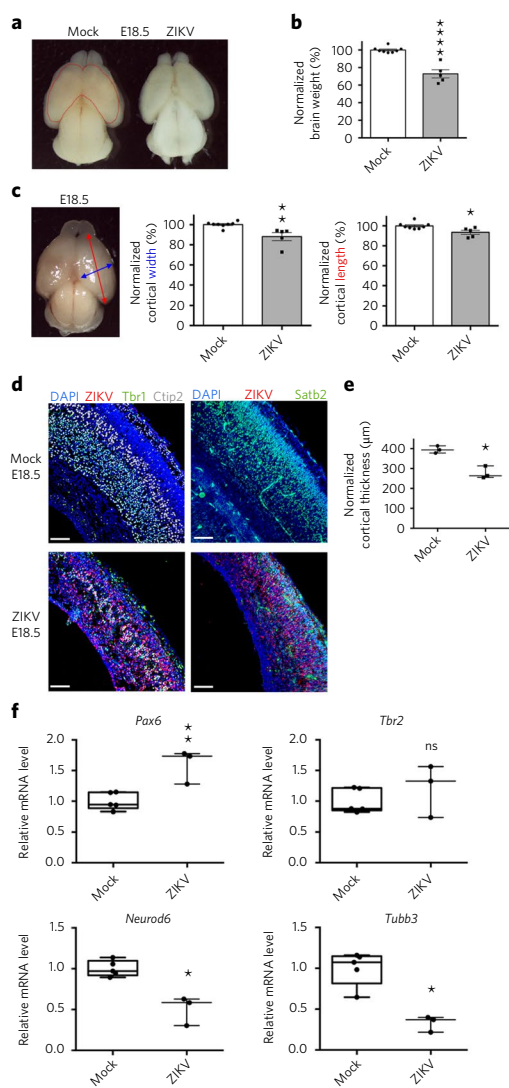


Fig. 2 | ICV injection of ZIKV induces microcephaly in mouse embryos.

a–e. Analyses of mock- or ZIKV-infected E18.5 mouse embryos brains. **(a)** Dorsal view of E18.5 mouse brains after ICV injection of mock (left; representative example from $n = 8$ brains from three to four dams) or ZIKV (right; representative example from $n = 5$ brains from three to four dams) at E12.5. Dotted red line corresponds to boundary of the ZIKV-infected cortex. **(b,c)** Analysis of morphological parameters between mock ($n = 8$) and ZIKV-infected ($n = 5$) E18.5 brains by unpaired two-tailed Student's *t* test, which shows **(b)** normalized brain weight (**** $P < 0.0001$, $t_{11} = 6.932$) and **(c)** normalized cortical width (** $P = 0.0042$, $t_{11} = 3.590$; blue double-headed arrow in the photograph) and length (* $P = 0.0137$, $t_{11} = 2.929$; red double-headed arrow). Data are presented as histograms and error bars of mean \pm s.e.m.; each symbol represents one embryo. **(d)** Immunolabeling comparing expression of DAPI (blue), ZIKV (red) and the neuronal layer markers *Tbr1* or *Satb2* (green) or *Ctip2* (gray) between mock- or ZIKV-infected cortices of E18.5 embryos. Scale bars, 100 μ m. **(e)** One-sided Mann-Whitney test comparing cortical thickness between mock-infected ($n = 3$) and ZIKV-infected ($n = 3$) E18.5 brains (* $P < 0.05$, $U = 0$). Boxplot shows median \pm first and third quartiles; whiskers extend to maxima and minima. **f.** qRT-PCR performed on total RNA extracts from mock- or ZIKV-infected E18.5 cortices to detect markers for APs and IPs, *Pax6* (** $P < 0.01$, $U = 0$) and *Tbr2* ($P = 0.5714$, $U = 5$), respectively, and the neuronal markers *NeuroD6* (* $P = 0.0357$, $U = 0$) and *Tubb3* (* $P = 0.0357$, $U = 0$). Data are analyzed by two-sided Mann-Whitney test and presented as boxplots showing median \pm first to third quartiles; whiskers extend to maxima and minima, and each symbol represents $n = 3$ –5 independent embryonic brain as indicated on respective boxplots. **** $P < 0.0001$, ** $P < 0.01$, * $P < 0.05$; ns, not significant.

ER-derived structures termed viral replication factories^{19–22}, we hypothesized that ZIKV replication may trigger an ER stress and upregulate UPR, thereby impairing indirect neurogenesis and contributing to microcephaly. Comparison of published gene-expression profiles obtained from either ZIKV-infected brains or human cortical progenitors, as well as a genetic model of ER stress-induced microcephaly, supports the activation of UPR pathways by ZIKV (Supplementary Fig. 1b). Hence, we investigated whether ZIKV infection triggers microcephaly via ER stress induction by combining analyses of infected human fetal brains with data obtained in experimentally ZIKV-infected human neural stem cells (hNSCs) and embryonic mouse brains.

We performed quantitative real-time (qRT)-polymerase chain reaction (PCR) analyses of genes involved in the UPR pathways on extracted RNA from human occipital cortices of two microcephalic ZIKV-infected fetuses in the second trimester (ZIKV#1 and ZIKV#2, 22 gestational weeks or GW), and of three uninfected (wild-type, WT) fetuses of comparable gestational ages (21 GW, 23 GW, and 24 GW; Fig. 1a). The expression of ZIKV in the brains of infected fetuses was confirmed by in situ hybridization (see representative image of ZIKV#1 in Supplementary Fig. 1c,d). In contrast to uninfected fetuses, ZIKV-infected cortices exhibited an upregulation of the gene encoding myxovirus resistance proteins (*MX1*; Fig. 1a), which is reported to be induced upon viral infection^{23,24}, as well as molecular components of the ER stress pathway and the PERK–ATF4 arm of UPR (Fig. 1a). Together, these results suggest that ZIKV induces ER stress and triggers UPR in cortical progenitors of fetuses during pregnancy.

To experimentally test this hypothesis, we infected cultured hNSCs²⁵, which display features of cortical progenitors (Supplementary Fig. 1e,f), with ZIKV (strain H/PF/2013) for 2 h and analyzed the ER stress and UPR molecular signatures 48 h later by qRT-PCR and immunocytochemistry (Fig. 1b–g). We detected ZIKV RNA in infected hNSCs and observed increased immunolabeling for the ER stress markers calnexin and calreticulin^{26,27} in these cells, in contrast to most uninfected (mock) hNSCs (Fig. 1c–f), concomitant with upregulation of *MX1* and the ER stress marker protein disulfide isomerase (PDI; Fig. 1g). Genes of the PERK–ATF4 arm of UPR were upregulated upon infection (Fig. 1g), as seen also upon tunicamycin treatment (Supplementary Fig. 1g). Moreover, the increased ratio of spliced/unspliced *XBP1* showed activation of the IRE-1 pathway upon ZIKV infection (Fig. 1g). Together, these findings directly support that ZIKV triggers ER stress and UPR in hNSCs.

In vivo injection of ZIKV induces microcephaly with activation of ER stress and UPR in mice. To corroborate these findings in vivo, ZIKV particles were intracerebroventricularly (ICV) injected into the forebrains of mice at embryonic day (E) 12.5, and brains were analyzed at E18.5. Infected mouse brains were microcephalic (Fig. 2a) and were significantly lighter (Fig. 2b), with smaller cortical dimensions (Fig. 2c), when compared to mock-injected embryos. Similar results were obtained in newborn pups injected at E12.5 (Supplementary Fig. 2a). Notably, the cortical thickness of ZIKV-infected brains was significantly reduced (Fig. 2d,e). Furthermore, ZIKV-infected brains exhibited a strong reduction of deeper neurons (Fig. 2d; *Tbr1*⁺ or *Ctip2*⁺ neurons) and upper-layer neurons (Fig. 2d; *Satb2*⁺ neurons), as well as a severe disruption in their laminar organization, compared to uninfected brains (Fig. 2d). Microdissected cortices from ZIKV-infected embryos showed an upregulation of the AP marker *Pax6* but not of the intermediate progenitor (IP) marker *Tbr2* (Fig. 2f). The upregulation of *Pax6* reflected the proportional increase in *Pax6*⁺ progenitors in the cortical wall upon ZIKV infection (Supplementary Fig. 2b–d). We also observed an overall relative reduction of expression of neuronal markers (Fig. 2f). These findings indicate the depletion of cortical neurons. We next investigated ER stress in ZIKV-infected cortical

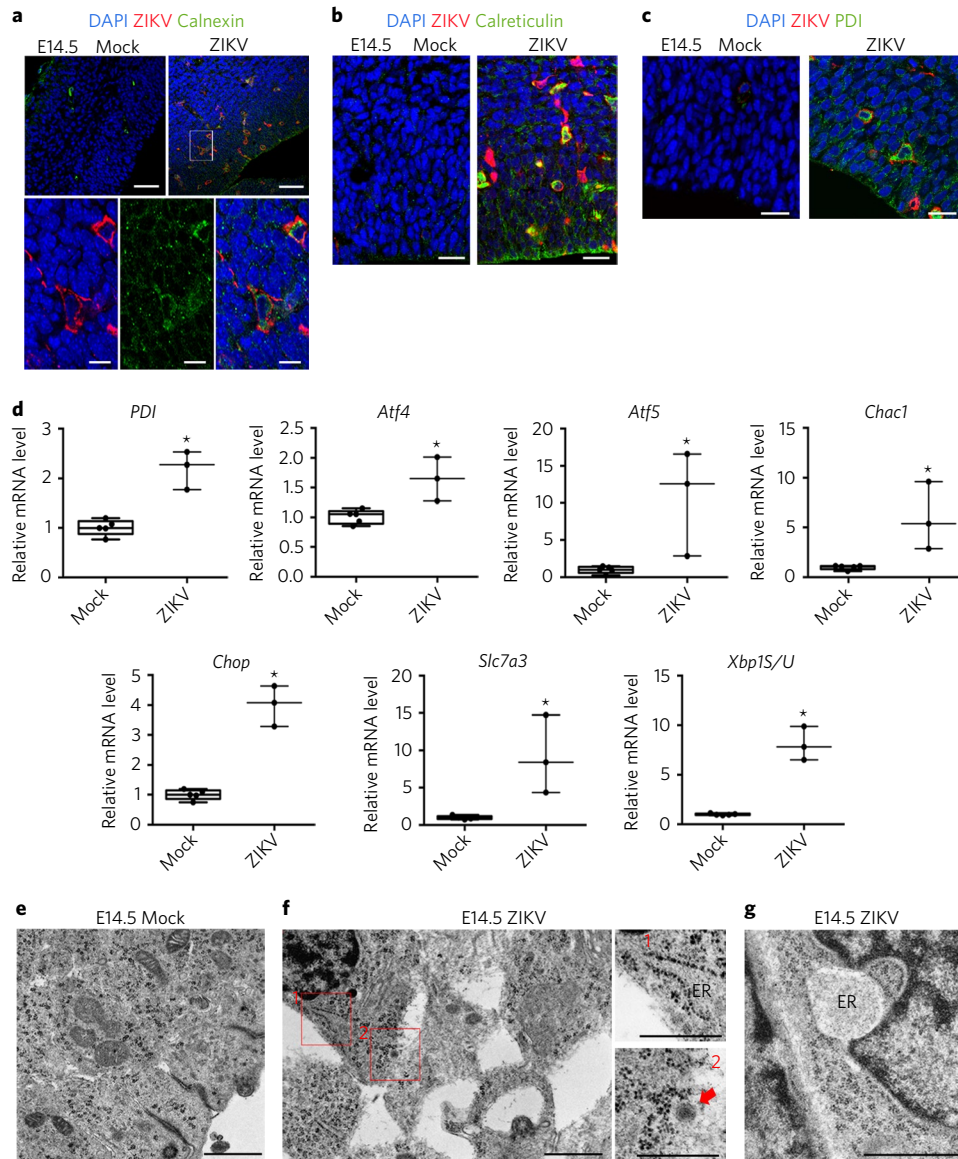


Fig. 3 | ICV injection of ZIKV induces activation of ER stress and UPR in mouse embryonic brains. **a–c**, Immunolabeling of mock-treated ($n=5$) or ZIKV-infected ($n=5$) E14.5 brains showing DAPI (blue), ZIKV (red) and the ER stress markers (**a**) calnexin (green), (**b**) calreticulin (green) or (**c**) PDI (green). Bottom row of **a** shows enlargements of the white boxed area in different channels: DAPI and ZIKV (bottom left), calnexin alone (bottom middle) and a merged image (bottom right). **d**, qRT-PCR performed on total RNA extracts from mock- or ZIKV-infected E18.5 cortices to detect ER stress or UPR actors, analyzed by two-sided Mann–Whitney test: *PDI* ($*P=0.0357$, $U=0$), *Atf4* ($*P=0.0357$, $U=0$), *Atf5* ($*P=0.0357$, $U=0$), *Chac1* ($*P=0.0357$, $U=0$), *Chop* ($*P=0.0357$, $U=0$), *Slc7a3* ($*P=0.0357$, $U=0$) and *Xbp1S/U* ($*P=0.0357$, $U=0$). Data presented as boxplots of median \pm first to third quartiles; whiskers extend to maxima and minima and each symbol represents $n=3$ –5 independent embryonic brains as indicated on boxplots. **e–g**, Transmission electronic micrographs of E14.5 mouse cortex that were ICV-injected with either mock ($n=3$) or ZIKV ($n=3$) medium at E12.5, showing an unaffected AP in the mock brain (**e**) and affected apical progenitors in ZIKV-infected brains (**f,g**); red arrow indicates a ZIKV particle; $n=3$ independent embryonic brains per condition). (**f**) AP from ZIKV-infected brain possesses an enlarged ER (red square 1) and a ZIKV particle (red square 2). (**g**) AP showing enlargement of the external nuclear membrane, which is continuous with the rough ER membrane system. Scale bars: $1\mu\text{m}$ in **e–g**, 500nm in **f** insets, $50\mu\text{m}$ in **b,c** and $100\mu\text{m}$ in **a** ($25\mu\text{m}$ in bottom row). We analyzed 3–5 brains per condition for all immunolabeling and histograms presented within this figure, and all embryos were taken from at least three separate litters per condition. $*P < 0.05$.

progenitors in coronal sections of E14.5 brains infected at E12.5. Congruent with our findings in ZIKV-infected hNSCs (Fig. 1b–g), we detected increased expression of ER stress markers in ZIKV-infected E14.5 cortices (Fig. 3a–c). In addition, qRT-PCR analyses confirmed ER stress induction, with upregulation of *Pdi* in ZIKV-infected cortical extracts from E18.5 mouse embryos (Fig. 3d). Moreover, in the same samples, we detected increased expression of key molecules of the UPR pathway, which has been shown to

control the neurogenic balance in the developing mouse cortex (Supplementary Fig. 1a)¹⁷. *Atf4* and its related targets (*Atf5*, *Chac1*, *Chop*, and *Slc7a3*) were significantly upregulated in ZIKV-infected cortices (Fig. 3d), as was the ratio of spliced/unspliced *Xbp1*, which also suggests an activation of the IRE-1 pathway (Fig. 3d). These data were supported by western blot analysis, which showed activation of the PERK pathway as well as a modest activation of the IRE-1 pathway (Supplementary Fig. 2e,f). We did not detect increased

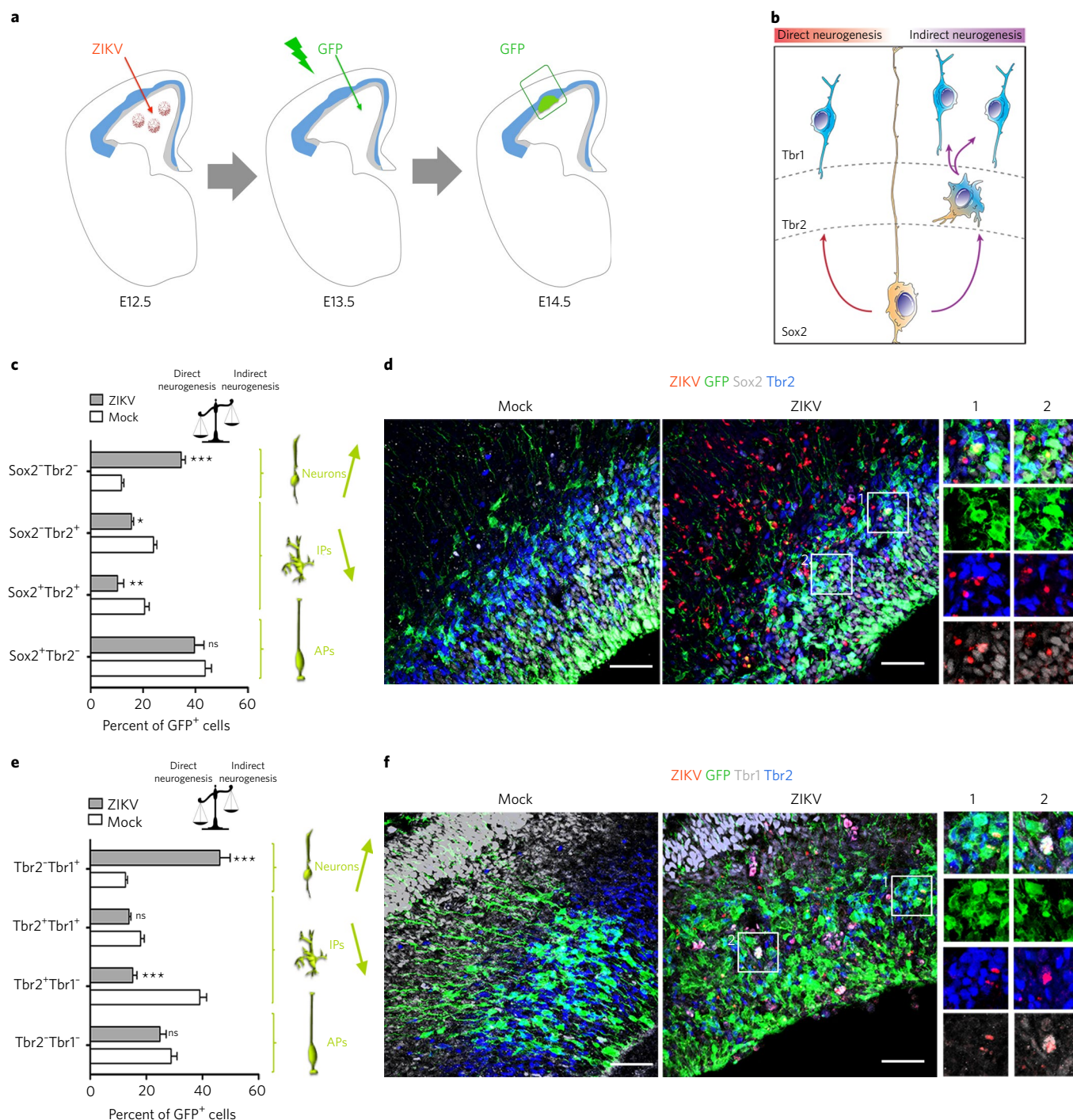


Fig. 4 | ICV injection of ZIKV promotes direct neurogenesis at the expense of indirect neurogenesis in mouse in vivo. **a**, Experimental strategy for tracking the first generation of E14.5 daughter cells of in utero-targeted E13.5 APs by GFP after ZIKV infection at E12.5. **b**, Electroporation of GFP in APs was performed 24 h before embryos were killed to assess their direct cellular progeny as APs (Sox2⁺Tbr2⁻ and Tbr2⁻Tbr1⁺), IPs (Sox2⁺Tbr2⁺ and Sox2⁻Tbr2⁺) or neurons (Sox2⁻Tbr2⁻ and Tbr2⁻Tbr1⁺). **c–f**, Assessment of the neurogenic balances upon mock treatment or ZIKV infection. **(c)** Percentages of cell expressing Sox2, Tbr2 or both in GFP⁺ cells. Data are presented as histograms and error bars of mean ± s.e.m. and analyzed by two-way ANOVA followed by Bonferroni post hoc comparison test ($F_{3,24} = 39.52$, $***P < 0.001$). **(d)** Immunolabeling of cortical sections from mock- or ZIKV-infected ($n = 5$ independent brains per condition) E14.5 embryos to detect ZIKV (red), GFP (green), Sox2 (light gray) and Tbr2 (blue) in APs (Sox2⁺Tbr2⁻), newborn IPs (Sox2⁺Tbr2⁺), IPs (Sox2⁻Tbr2⁻) and neurons (Sox2⁻Tbr2⁻). Insets: area 1 shows a Sox2⁺Tbr2⁺ newborn IP; area 2 shows a Sox2⁻Tbr2⁻ neuron. **(e)** Percentages of cell expressing Tbr2, Tbr1 or both in GFP⁺ cells. Data are presented as in **c** ($F_{3,32} = 113.34$, $***P < 0.001$). **(f)** Immunolabeling of cortical sections from mock- or ZIKV-infected E14.5 embryos to detect ZIKV (red), GFP (green), Tbr1 (gray) and Tbr2 (blue) in APs (Tbr2⁻Tbr1⁻), newborn IPs (Tbr2⁺Tbr1⁺), IPs (Tbr2⁺Tbr1⁺) and neurons (Tbr2⁻Tbr1⁺). Area 1 shows a Tbr1⁺Tbr2⁺ newborn IP; area 2 shows a Tbr1⁺Tbr2⁻ neuron. We analyzed five E14.5 brains per condition for all immunolabeling and histograms presented within this figure, and all embryos were taken from at least three separate litters per condition. Scale bars represent 50 μm in **d** and **f**. $***P < 0.001$, $**P < 0.01$, $*P < 0.05$; ns, not significant.

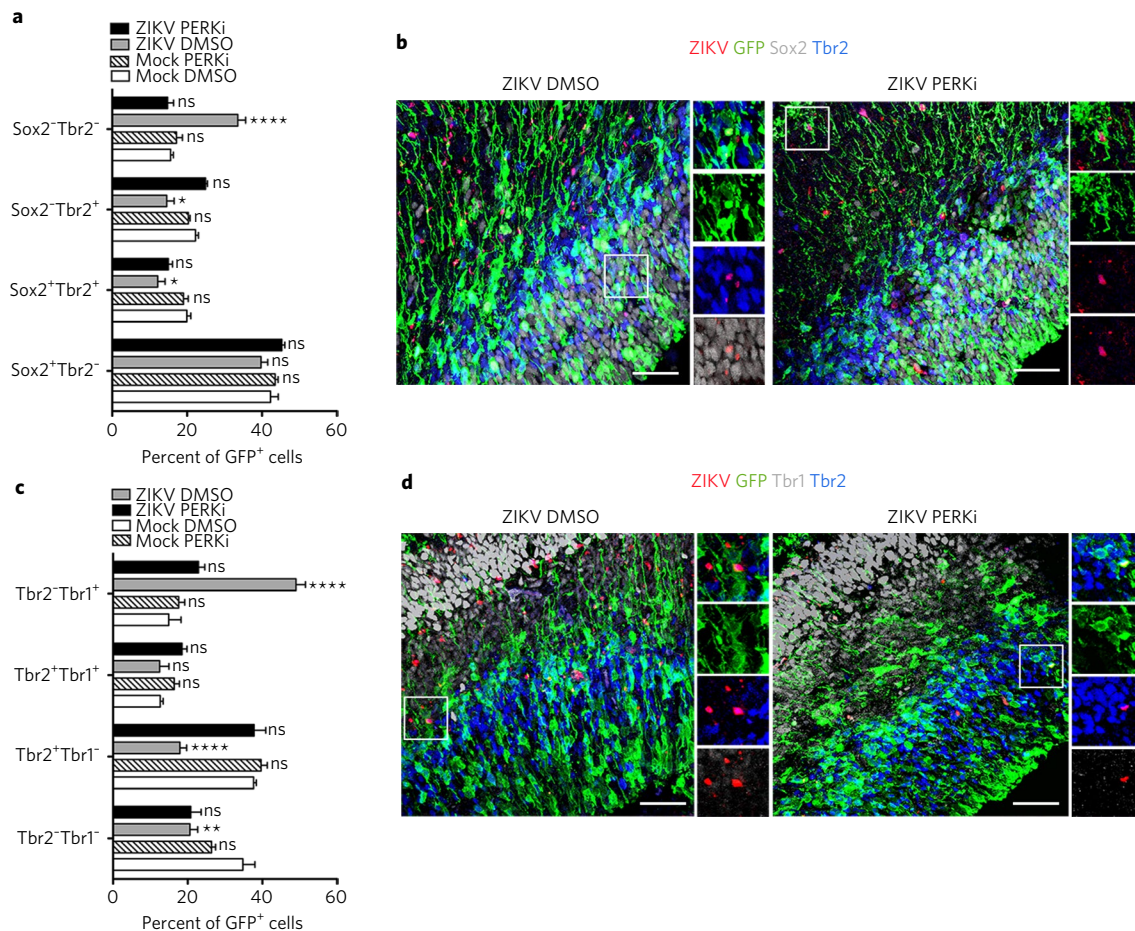


Fig. 5 | PERKi rescues the neurogenic balance upon ICV injection of ZIKV in mouse in vivo. Assessment of the neurogenic balances upon mock treatment or ZIKV infection with or without PERKi. **a**, Percentages of cell expressing Sox2, Tbr2 or both in GFP⁺ cells, analyzed by two-way ANOVA followed by Bonferroni post hoc comparison test ($F_{9,64} = 25.47$, $***P < 0.001$). Error bars show mean \pm s.e.m. **b**, Immunolabeling of cortical sections from mock- or ZIKV-infected ($n = 5$ brains per condition) E14.5 embryos treated or not with PERKi to detect ZIKV (red), GFP (green), Sox2 (light gray) and Tbr2 (blue) in APs (Sox2⁻Tbr2⁻), newborn IPs (Sox2⁺Tbr2⁺), IPs (Sox2⁻Tbr2⁺) and neurons (Sox2⁺Tbr2⁻). Left insets show a Sox2⁺Tbr2⁻ AP; right insets show a Sox2⁻Tbr2⁺ neuron. **c**, Percentages of cell expressing Tbr2, Tbr1 or both in GFP⁺ cells ($F_{9,64} = 65.59$, $***P < 0.001$), analyzed by two-way ANOVA followed by Bonferroni post hoc comparison test. Error bars show mean \pm s.e.m. **d**, Immunolabeling of cortical sections from mock- or ZIKV-infected E14.5 embryos treated or not by PERKi to detect ZIKV (red), GFP (green), Tbr1 (gray) and Tbr2 (blue) in APs (Tbr2⁻Tbr1⁻), newborn IPs (Tbr2⁺Tbr1⁺), IPs (Tbr2⁺Tbr1⁻) and neurons (Tbr2⁻Tbr1⁺). Left insets show a Tbr1⁻Tbr2⁻ AP; right insets show a Tbr1⁻Tbr2⁺ immature IP. Five E14.5 brains per condition were analyzed for all immunolabeling and histograms presented within this figure, and all embryos were taken from at least three separate litters per condition. Scale bars, 50 μ m. $****P < 0.0001$, $***P < 0.001$, $**P < 0.01$, $*P < 0.05$; ns, not significant.

cleavage of ATF6 or upregulation of its target, *Xbp1* (data not shown). Similar observations were made in a mouse model of ZIKV maternal–fetal vertical transmission¹⁰; E14.5 embryonic cortices collected from *Ifnar1*^{-/-} pregnant dams infected intraperitoneally at gestational day 9.5 showed also upregulation of markers of the UPR pathway (Supplementary Fig. 2g). Moreover, unlike in utero mock-injected embryos (Fig. 3e), transmission electronic micrographs of E14.5 cortical APs from ZIKV-infected embryos showed signs of ER stress (Fig. 3f,g). Altogether, these results indicate that ZIKV infection induces ER stress and an elevation of the UPR in mouse APs in vivo.

Intracerebroventricular injection of ZIKV promotes direct neurogenesis at the expense of indirect neurogenesis in mouse. We have previously shown that disrupting the physiological regulation of UPR in cerebral cortical APs causes microcephaly by promoting direct neurogenesis at the expense of indirect neurogenesis¹⁷ (Supplementary Fig. 1a). While some projection neurons are

generated from APs via direct neurogenesis, most of them arise via indirect neurogenesis, after division of IPs²⁸. To test whether the deregulation of UPR induced by ZIKV infection results in the impairment of the neurogenic balance, we performed ICV injection of ZIKV in E12.5 mouse brains, followed by in utero electroporation of GFP in APs. To fate-map their direct progenies (APs, IPs, immature IPs and neurons), we assessed the expression of cell fate markers 24h after the electroporation of GFP in APs (a time period shorter than two AP cell cycles, thereby allowing the identification of their direct progenies; Fig. 4a,b). The phenotype of the ‘direct progeny’ of targeted APs was assessed by immunohistochemistry (Fig. 4d–f). To characterize the fate of GFP⁺ cells, we subdivided them into APs (Sox2⁺Tbr2⁻ or Tbr2⁻Tbr1⁻; Fig. 4d), immature IPs (Sox2⁺Tbr2⁺ or Tbr2⁺Tbr1⁻; Fig. 4f), IPs (Sox2⁻Tbr2⁺ or Tbr2⁺Tbr1⁺) or neurons (Sox2⁻Tbr2⁻ or Tbr2⁻Tbr1⁺; Fig. 4d,f). Analyses of ZIKV-infected GFP⁺ APs (as detected by anti-NS1 antibodies and similarly to the anti-flavivirus group antigen, antibody 4G2; Supplementary Fig. 3a,b) showed that the majority of GFP⁺

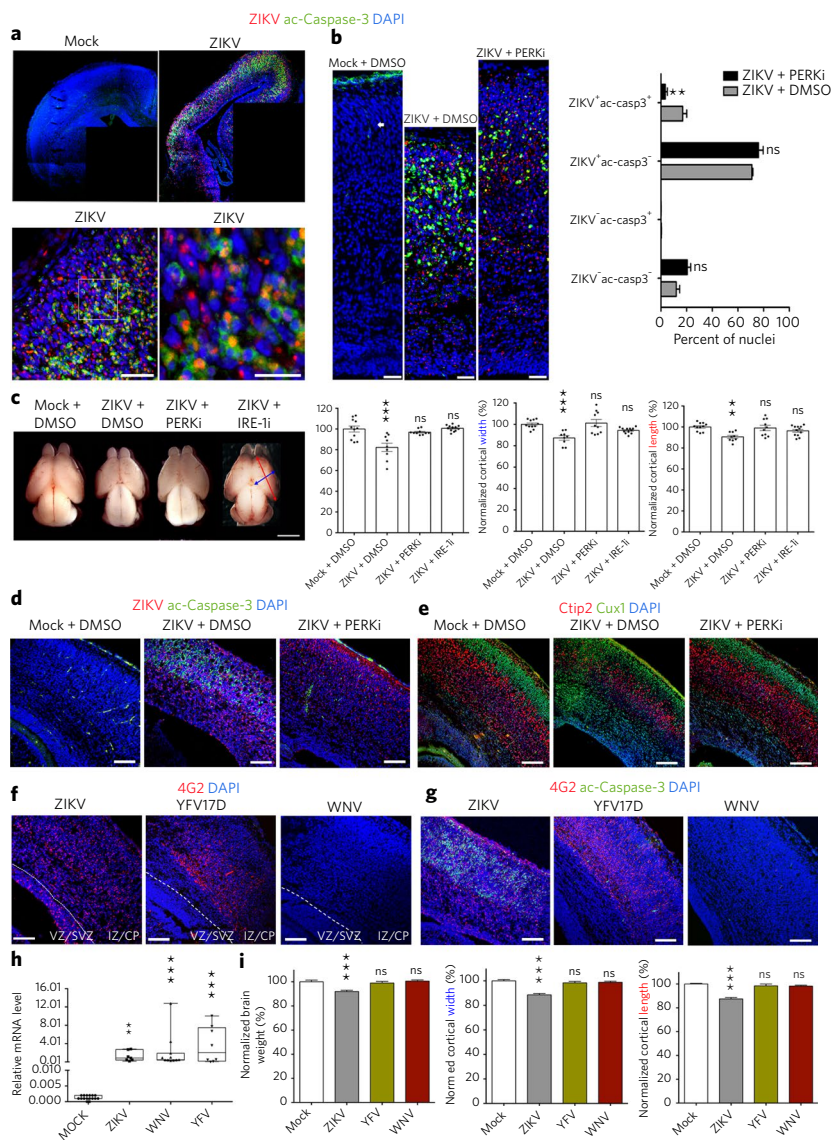


Fig. 6 | ICV and intraplacental (IPL) injection of ZIKV, but not yellow fever (YFV) or WNV viruses, induces microcephaly and cell death in mouse brains.

a, Cell death in E18.5 brains after mock or ZIKV infection at E12.5. Top: immunolabeling of E18.5 coronal sections after mock treatment or ZIKV infection at E12.5 showing DAPI (blue), ZIKV (red) and ac-caspase-3 (green); $n=3$ independent embryonic brains per condition. Bottom: higher magnifications of ZIKV-infected cortex (right image is an enlargement of the white squared area in the left image). **b,c**, ICV coinjection of ZIKV with either PERKi or IRE-1i pathway rescues microcephaly. **(b)** Immunolabeling of E18.5 coronal sections showing DAPI (blue), ZIKV (red) and ac-caspase-3 (ac-casp3, green; $n=5$ independent embryonic brains per condition) after mock treatment (6 brains), ZIKV infection (7 brains) or ZIKV + PERKi (7 brains) at E12.5 (from at least 3 separate litters per condition). Histograms show data analyzed by one-way ANOVA followed by Bonferroni post hoc comparison test, comparing the percentages of cells coexpressing ZIKV and ac-caspase-3 ($F_{9,161} = 8.320$, $***P < 0.001$). Error bars show mean \pm s.e.m. **(c)** Dorsal view of representative E18.5 mouse brains after mock treatment, ZIKV infection, ZIKV + PERKi or ZIKV + IRE-1i at E12.5. Data are presented as histograms analyzed by one-way ANOVA followed by Bonferroni post hoc comparison test to compare morphological parameters of E18.5 brains after injection of mock ($n=10$ brains), ZIKV ($n=9$ brains), ZIKV + PERKi ($n=10$ brains) or ZIKV + IRE-1i ($n=12$ brains) at E12.5, normalized brain weight ($F_{3,38} = 12.14$, $***P < 0.001$), cortical width ($F_{3,38} = 9.441$, $***P < 0.001$; blue double-headed arrow in the rightmost brain image) and length ($F_{3,38} = 5.76$, $**P = 0.0024$; red double-headed arrow in rightmost brain). **d-i**, IPL injection of ZIKV phenocopies E18.5 cortical defects induced by ICV infection at E12.5, while IPL coinjection of PERKi rescues microcephaly. Immunolabeling of E18.5 coronal sections after IPL injection of mock ($n=3$ brains), ZIKV ($n=3$ brains), or ZIKV + PERKi ($n=4$ brains) at E12.5 showing **(d)** DAPI (blue), ZIKV (red) and ac-caspase-3 (green) or **(e)** DAPI (blue), Cux1 (green) and Ctip2 (red). **(f-i)** Analyses of E18.5 mouse brains after IPL injection of ZIKV, YFV17D or WNV at E12.5. Immunolabeling of E18.5 coronal sections with **(f)** DAPI (blue) and 4G2 (pan-flaviviral antibody, red) or **(g)** DAPI (blue), 4G2 (red) and ac-caspase-3 (green); $n=3$ embryonic brains per condition. **(h)** qRT-PCR performed on total RNA extract from placentas of embryos injected with ZIKV, YFV17D or WNV to detect expression of respective flavivirus. Data are presented as boxplots (median \pm first to third quartiles; whiskers extend to maxima and minima; each symbol represents $n=8-16$ placentas as indicated) analyzed by Kruskal-Wallis ANOVA followed by Dunn post hoc comparison test ($F_{3,39} = 29.44$, $***P < 0.001$). **(i)** Analysis of morphological parameters of E18.5 brains after intraplacental injection with ZIKV, YFV17D or WNV at E12.5 ($n=13$, 21 and 13 independent embryonic brains, respectively, from at least three separate litters per condition) by one-way ANOVA followed by Bonferroni post hoc comparison test, comparing normalized brain weight ($F_{3,55} = 8.394$, $***P < 0.001$), cortical width ($F_{3,55} = 20.86$, $***P < 0.001$; blue double-headed arrow in **c**) and cortical length ($F_{3,55} = 32.66$, $***P < 0.0001$; red double-headed arrow in **c**) of E18.5 brains. Error bars indicate mean \pm s.e.m. $***P < 0.001$, $**P < 0.01$; ns, not significant. VZ/SVZ, ventricular zone and subventricular zone; IZ/CP, intermediate zone and cortical plate. Scale bars, 30 μ m in **a**, 50 μ m in **b**, 200 μ m in **c** and 100 μ m in **d-g**.

ZIKV-infected cells were proliferating (65.8 ± 9.6 ; $n = 5$ brains; mean \pm s.e.m.) and, compared to GFP⁺ cells in uninfected brains, gave rise to a significantly lower proportion of IPs and a higher proportion of neurons, without reducing the fraction of self-renewing APs (Fig. 4c–e) or the rate of cell proliferation in infected cortices at E14.5 (Supplementary Figs. 3c,d and 4a). Altogether, these results show that in vivo infection of APs by ZIKV directly impacts cortical neurogenesis by shifting the balance toward direct neurogenesis at the expense of indirect neurogenesis, thereby reducing the overall projection neuron output. Notably, ZIKV also impairs the neurogenic balance through non-cell-autonomous mechanisms (Supplementary Fig. 4b).

ZIKV-induced neurogenic defect is rescued by inhibition of the PERK arm of the upregulated UPR pathway in mouse. To assess whether ZIKV directly impacts the neurogenic balance through UPR deregulation in GFP-labeled APs, we coinjected GSK2656157 (a PERK inhibitor, hereafter referred to as ‘PERKi’) ²⁹ with ZIKV into the lateral ventricles of E12.5 embryos and gave a second PERKi injection at the time of electroporation (E13.5). Treatment with PERKi (10 μ M, solubilized in dimethyl sulfoxide, DMSO) did not perturb the neurogenic balance, as no significant differences were detected in different cellular compartments between brains treated with mock + DMSO and those treated with mock + PERKi. Moreover, administration of DMSO did not change the ability of ZIKV (ZIKV + DMSO) to impair neurogenesis as compared to control (mock + DMSO; Fig. 5a–d). Coadministering PERKi with ZIKV corrected the imbalance between direct and indirect neurogenesis, rescuing the proportions of APs, newborn IPs, IPs and neurons to control levels at E14.5, when compared to mock + DMSO and mock + PERKi treatment (Fig. 5a–d and Supplementary Fig. 4b). Altogether, these data suggest that proper cortical neurogenesis can be restored in the context of ZIKV infection by chemically reducing the activation of UPR induced by ZIKV-associated ER stress.

In vivo inoculation of ZIKV, but not related flaviviruses, induces microcephaly and apoptosis in mouse brains. Although an increase of UPR can also lead to apoptosis ³⁰, we did not observe a reduction of cell survival at E14.5 (Supplementary Fig. 4c) and only detected significant neuronal apoptosis later at E18.5 in ZIKV brains infected at E12.5 (Fig. 6a and Supplementary Fig. 4d), concomitant with elevated PDI expression (Supplementary Fig. 4e). While detailed analysis revealed that only a fraction of ZIKV-expressing neurons was apoptotic (Fig. 6b), no significant apoptosis was observed in the progenitor region of the cortex, likely because ZIKV favors the generation of neurons that exit this region (Fig. 4c,e) ¹³. Indeed, most dying cells were observed in the postmitotic regions of the cortex (Fig. 6b), and a single injection of 50 μ M PERKi at the time of infection (E12.5) decreased ER stress (Supplementary Fig. 4f,g) and apoptosis (Fig. 6b). Strikingly, injection of PERKi reduced ZIKV-induced microcephaly (Fig. 6c), as supported by the significant improvement of brain weight, cortical dimensions and number of neurons in different cortical layers (Supplementary Fig. 5a,b) compared to vehicle treatment. Since increased splicing of *Xbp1* was also detected in ZIKV-infected hNSCs and mouse brains (Figs. 1g and 3d), we also injected an inhibitor of IRE-1, 4 μ 8 C (IRE-1i). This rescued the microcephaly phenotype to a similar extent compared to PERKi (Fig. 6c). IRE-1i also prevented activation of the PERK–ATF4 UPR arm (Supplementary Fig. 4h), suggesting a potential crosstalk between the two UPR pathways ^{31,32}. While PERKi displays no antiviral effect on ZIKV, as it is not associated with a reduction of the number of cortical cells infected by ZIKV (Supplementary Fig. 4i) or the number of ZIKV particles detected in extracts from cortical samples (Supplementary Fig. 4j), the IRE-1i-mediated rescue may also partly result from impaired ZIKV replication (Supplementary

Fig. 4j). Our data thus suggest that the predominant mechanism of ZIKV-induced microcephaly is the impairment of a physiological UPR that controls the balance between direct and indirect neurogenesis and whose disruption reduces the neuronal output as well as long-term neuronal survival.

To model the natural ZIKV infection pathway ¹¹, we injected viral particles into the placenta of NMRI mice at E12.5 ³³. Similarly to ICV infection (Fig. 2d,e), E12.5 intraplacental injection of ZIKV led to reduction of cortical thickness at E18.5, together with ER stress induction (Supplementary Fig. 5c), massive neuronal apoptosis (Fig. 6b) and impairment of cortical cytoarchitecture (Fig. 6e). These ZIKV-induced cortical defects were rescued by coinjection of PERKi.

To investigate whether the tropism for APs and the capability to cross the embryonic blood–brain barrier is unique to ZIKV, we intraplacentally injected either the neurotropic strain of yellow fever virus ¹⁰ (vaccine strain 17D or YFV17D) or West Nile virus (WNV), two closely related flaviviruses. Although all three flaviviruses efficiently infected the placental tissue (Fig. 6h), YFV17D and WNV neither infected APs, triggered apoptosis nor induced microcephaly (Fig. 6f–i). Of note, YFV17D exhibits a tropism for cells in the intermediate zone and cortical plate, which are predominantly postmitotic neurons (Fig. 6g).

Discussion

The formation of the cerebral cortex involves successive waves of neurons whose generation is finely regulated. At the onset of corticogenesis, neurons are predominantly born directly via asymmetric division of APs. Later, APs produce IPs, which further divide symmetrically to generate the bulk of projection neurons via a process termed indirect neurogenesis. The neurogenesis balance (direct versus indirect) is dynamically regulated during development by a physiological UPR whose disruption leads to microcephaly ¹⁷. ZIKV, which has been recently associated with microcephaly in humans ^{8,9}, targets cortical APs in vivo ^{12,13,15,18}.

Our study showed ER stress and UPR activation both in post-mortem cortical samples from ZIKV-infected human fetuses and in cultured human neural stem cells. Furthermore, our in vivo experiments in mouse embryos demonstrated vertical transmission of ZIKV and confirmed its selective targeting of cortical APs. In stark contrast to previous studies reporting apoptotic death of neural progenitors in vitro ^{15,34}, we did not observe apoptosis of ZIKV-infected APs. Moreover, infection of APs did not interfere with their proliferation but rather with their ability to generate IPs, hence leading to reduced neuronal output in the infected developing cortex.

Additionally, the neurogenic defect was also detected in noninfected ZIKV APs, either due to a non-cell-autonomous mechanism or suggesting that the level of infection was below the threshold of immunodetection. Notably, these defects were rescued by inhibition of PERK in ZIKV-positive and ZIKV-negative cortical cells.

Infected neurons rapidly exit the progenitor regions to invade the cortical plate, a process that may also involve the destabilization of adherens junction complexes by ZIKV-encoded nonstructural proteins ³⁵. The sustained ER stress in infected projection neurons subsequently triggers terminal UPR and apoptosis via upregulation of *Chop* in vivo (Supplementary Fig. 5d–f). Altogether, our data indicates that ZIKV-induced ER stress and UPR deregulation contribute to microcephaly via reduced neuronal output from APs and by enhancing susceptibility of their neuronal progeny to terminal UPR-dependent apoptosis (Supplementary Fig. 5g).

UPR is mediated by three pathways, and we demonstrated that direct inhibition of the PERK-mediated UPR pathway in ZIKV-infected brains rescues the neurogenic balance and prevents terminal UPR-induced apoptosis, thereby preventing microcephaly. Furthermore, inhibition of the IRE-1a-mediated UPR also rescued ZIKV-induced microcephaly in mouse embryos. Inhibiting IRE-1a reduces ZIKV replication, but also downregulates *Atf4*,

which is a direct target of the PERK pathway. Altogether, these results suggest that deregulation of *Atf4* is a predominant driver of ZIKV-induced microcephaly.

We report that infection by ZIKV, but not YFV17D or WNV, contributes to microcephaly via a specific cascade of events: (i) vertical transmission of virus, (ii) targeting of APs and (iii) induction of ER stress and activation of UPR in APs and neurons. The infection of mouse organotypic cultures by WNV has suggested its possible tropism for cortical cells³⁶. However, using intraplacental injection of WNV, we show that it did not cross the embryonic blood–brain barrier to reach the developing cortex *in vivo*. We conclude that targeting UPR activation by inhibitors stands as a potential therapeutic approach aimed at lowering ZIKV-associated neuropathogenesis in the developing cortex.

Methods

Methods, including statements of data availability and any associated accession codes and references, are available at <https://doi.org/10.1038/s41593-017-0038-4>.

Received: 11 August 2017; Accepted: 14 November 2017;

Published online: 11 December 2017

References

- Gupta, A., Tsai, L. H. & Wynshaw-Boris, A. Life is a journey: a genetic look at neocortical development. *Nat. Rev. Genet.* **3**, 342–355 (2002).
- Rash, B. G. & Grove, E. A. Area and layer patterning in the developing cerebral cortex. *Curr. Opin. Neurobiol.* **16**, 25–34 (2006).
- Laguette, S., Peyre, E. & Nguyen, L. Progenitor genealogy in the developing cerebral cortex. *Cell Tissue Res.* **359**, 17–32 (2015).
- Sarnat, H. B. & Flores-Sarnat, L. A new classification of malformations of the nervous system: an integration of morphological and molecular genetic criteria as patterns of genetic expression. *Eur. J. Paediatr. Neurol.* **5**, 57–64 (2001).
- Sarnat, H. B. & Flores-Sarnat, L. Neuroembryology and brain malformations: an overview. *Handb. Clin. Neurol.* **111**, 117–128 (2013).
- Woods, C. G. & Parker, A. Investigating microcephaly. *Arch. Dis. Child.* **98**, 707–713 (2013).
- Cauchemez, S. et al. Association between Zika virus and microcephaly in French Polynesia, 2013–15: a retrospective study. *Lancet* **387**, 2125–2132 (2016).
- Driggers, R. W. et al. Zika virus infection with prolonged maternal viremia and fetal brain abnormalities. *N. Engl. J. Med.* **374**, 2142–2151 (2016).
- Mlakar, J. et al. Zika virus associated with microcephaly. *N. Engl. J. Med.* **374**, 951–958 (2016).
- Cugola, F. R. et al. The Brazilian Zika virus strain causes birth defects in experimental models. *Nature* **534**, 267–271 (2016).
- Miner, J. J. et al. Zika virus infection during pregnancy in mice causes placental damage and fetal demise. *Cell* **165**, 1081–1091 (2016).
- Li, C. et al. Zika virus disrupts neural progenitor development and leads to microcephaly in mice. *Cell Stem Cell* **19**, 120–126 (2016).
- Onorati, M. et al. Zika virus disrupts phospho-TBK1 localization and mitosis in human neuroepithelial stem cells and radial glia. *Cell Rep.* **16**, 2576–2592 (2016).
- Qian, X. et al. Brain-region-specific organoids using mini-bioreactors for modeling ZIKV exposure. *Cell* **165**, 1238–1254 (2016).
- Tang, H. et al. Zika virus infects human cortical neural progenitors and attenuates their growth. *Cell Stem Cell* **18**, 587–590 (2016).
- Wu, K. Y. et al. Vertical transmission of Zika virus targeting the radial glial cells affects cortex development of offspring mice. *Cell Res.* **26**, 645–654 (2016).
- Laguette, S. et al. A dynamic unfolded protein response contributes to the control of cortical neurogenesis. *Dev. Cell* **35**, 553–567 (2015).
- Chavali, P. L. et al. Neurodevelopmental protein Musashi-1 interacts with the Zika genome and promotes viral replication. *Science* **357**, 83–88 (2017).
- Bell, T. M., Field, E. J. & Narang, H. K. Zika virus infection of the central nervous system of mice. *Arch. Gesamte. Virusforsch.* **35**, 183–193 (1971).
- Hamel, R. et al. Biology of Zika virus infection in human skin cells. *J. Virol.* **89**, 8880–8896 (2015).
- Monel, B. et al. Zika virus induces massive cytoplasmic vacuolization and paraptosis-like death in infected cells. *EMBO. J.* **36**, 1653–1668 (2017).
- Paul, D. & Bartenschlager, R. Flaviviridae replication organelles: oh, what a tangled web we weave. *Annu. Rev. Virol.* **2**, 289–310 (2015).
- Pillai, P. S. et al. Mx1 reveals innate pathways to antiviral resistance and lethal influenza disease. *Science* **352**, 463–466 (2016).
- Staeli, P., Haller, O., Boll, W., Lindenmann, J. & Weissmann, C. Mx protein: constitutive expression in 3T3 cells transformed with cloned Mx cDNA confers selective resistance to influenza virus. *Cell* **44**, 147–158 (1986).
- Borgs, L. et al. Dopaminergic neurons differentiating from LRRK2 G2019S induced pluripotent stem cells show early neuritic branching defects. *Sci. Rep.* **6**, 33377 (2016).
- Bernard-Marissal, N. et al. Reduced calreticulin levels link endoplasmic reticulum stress and Fas-triggered cell death in motoneurons vulnerable to ALS. *J. Neurosci.* **32**, 4901–4912 (2012).
- Olgar, Y., Ozdemir, S. & Turan, B. Induction of endoplasmic reticulum stress and changes in expression levels of Zn(2+)-transporters in hypertrophic rat heart. *Mol. Cell. Biochem.* <https://doi.org/10.1007/s11010-017-3168-9> (2017).
- Sessa, A. et al. Tbr2-positive intermediate (basal) neuronal progenitors safeguard cerebral cortex expansion by controlling amplification of pallial glutamatergic neurons and attraction of subpallial GABAergic interneurons. *Genes Dev.* **24**, 1816–1826 (2010).
- Axten, J. M. et al. Discovery of GSK2656157: an optimized PERK inhibitor selected for preclinical development. *ACS Med. Chem. Lett.* **4**, 964–968 (2013).
- Walter, P. & Ron, D. The unfolded protein response: from stress pathway to homeostatic regulation. *Science* **334**, 1081–1086 (2011).
- Gupta, A. et al. NCOA3 coactivator is a transcriptional target of XBP1 and regulates PERK-eIF2 α -ATF4 signalling in breast cancer. *Oncogene* **35**, 5860–5871 (2016).
- Tsuru, A., Imai, Y., Saito, M. & Kohno, K. Novel mechanism of enhancing IRE1 α -XBP1 signalling via the PERK-ATF4 pathway. *Sci. Rep.* **6**, 24217 (2016).
- Bonnin, A. et al. A transient placental source of serotonin for the fetal forebrain. *Nature* **472**, 347–350 (2011).
- Ghouzzi, V. E. et al. Zika virus elicits P53 activation and genotoxic stress in human neural progenitors similar to mutations involved in severe forms of genetic microcephaly and p53. *Cell Death Dis.* **7**, e2440 (2016).
- Yoon, K. J. et al. Zika-virus-encoded NS2A disrupts mammalian cortical neurogenesis by degrading adherens junction proteins. *Cell Stem Cell* **21**, 349–358.e6 (2017).
- Brault, J. B. et al. Comparative analysis between flaviviruses reveals specific neural stem cell tropism for Zika virus in the mouse developing neocortex. *EBioMedicine* **10**, 71–76 (2016).

Acknowledgements

The authors are thankful for technical help from the GIGA-Imaging Platform of ULg; M. Leruez-Ville for human sample collection; P.V. Drion, E.D. Valentin and C. Grignat for the flaviviral facility; C. d'Alessandro, M. Sambon and M. Lavina for technical assistance; E. Simon-Loriere for sharing ZIKV quantification protocol; and E. Peyre for graphical assistance. L.N., I.G.-N. and C.C. receive financial support from F.R.S.-FN.R.S. This work was supported by the European Union's Horizon 2020 Research and Innovation Programme under ZIKAlliance Grant Agreement N° 734548 (to L.N. and M.L.) and by the European Virus Archives goes Global (EVAg) project under grant agreement N° 653316. M.L. is also funded by Institut Pasteur, Inserm and LabEx IBEID. L.N. and P.V. are funded by F.R.S.-FN.R.S., the Fonds Léon Fredericq, the Fondation Médicale Reine Elisabeth, the Fondation Simone et Pierre Clerdent and the Belgian Science Policy (IAP-VII network P7/20). L.N. is funded by ARC (ARC11/16-01) and the ERANET Neuron STEM-MCD; P.V. is funded by the WELBIO Program of the Walloon Region, the AXA Research Fund, the Fondation ULB, ERANET Neuron Microkin, ERANET E-rare Euromicro and ERC-2013 ERC-2013-AG-340020.

Author contributions

I.G.-N., L.C.B., C.A., C.C., T.C., M.L. and L.N. designed the study. I.G.-N. set up animal models for ZIKV infection and, together with T.C., generated and analyzed *in vivo* data with help of G.M., L.C.B., M.A., C.A. and C.C. N.T. and M.T. performed and interpreted TEM analyses. L.C.B. generated data with hNSCs and performed analyses with help of C.A., I.G.-N. and C.C. C.A. and M.A. analyzed human brain samples provided by B.B., F.E.-R., M.B., I.S. and P.V. M.F. shared antibodies. L.N. contributed to data interpretation and wrote the manuscript with help from M.L. and input from all coauthors.

Competing interests

The authors declare no competing financial interests.

Additional information

Supplementary information is available for this paper at <https://doi.org/10.1038/s41593-017-0038-4>.

Reprints and permissions information is available at www.nature.com/reprints.

Correspondence and requests for materials should be addressed to M.L. or L.N.

Publisher's note: Springer Nature remains neutral with regard to jurisdictional claims in published maps and institutional affiliations.

Methods

Animals. Immunocompetent NMRI (Janvier Labs, Saint Berthevin, France) mice whose mating had been timed were housed under standard conditions, and all procedures were approved by the Animal Ethics Committee of the University of Liège (#16-1829) and performed in accordance with the guidelines of the Belgian Ministry of Agriculture, in agreement with the European Community Laboratory Animal Care and Use Regulations (86/609/CEE, Journal Officiel des Communautés Européennes L358, 18 December 1986). Mice in which the type I interferon (IFN) receptor gene was knocked out (IFN- α/β R^{-/-} mice) were housed in the Institut Pasteur animal facilities, which are accredited by the French Ministry of Agriculture for live rodent experimentation, and experiments involving them were approved by the Ethics Committee #89 and registered under the reference #2016-0018. All experiments on animals were performed in compliance with French and European regulations on care and protection of laboratory animals (EC Directive 2010/63, French Law 2013-118, February 6th, 2013).

Human fetal cortical samples. Human fetal brain material was obtained following medical pregnancy termination and processed as described in ref. ³⁷. Frontal and occipital cortex samples were dissected and flash-frozen in liquid nitrogen or Trizol at -80 °C. RNA was extracted using Total RNA kit I (Omega). The study was approved by all relevant ethics committees (Erasmus Hospital, Université Libre de Bruxelles, and Belgian National Fund for Scientific Research FRS/FNRS; French Agence de la Biomédecine, #PFS15-009) on research involving human subjects. Written informed consent was given by the parents of each donor.

RNA in situ hybridization. Nonradioactive RNA in situ hybridizations on frozen sections of a 25-GW human fetal brain (ZIKV#1) were performed as previously described³⁸ using digoxigenin-labeled sense and antisense riboprobes for ZIKV. The template was a PCR fragment amplified from ZIKV genome (GCF_000882815.3). The following primers were used to amplify the 3' UTR region of ZIKV: forward 5'-AGGTGAAGCACGGAGATCTAGAAG-3', reverse 5'-CCACTAACGTTCTTTGCAGACAT-3'. The riboprobes were synthesized by using the DIG labeling mix (Roche) according to manufacturer's instructions.

Immunohistochemistry. Embryonic (E) 14.5, E16.5 and E18.5 mouse brains were dissected in 0.1 M phosphate-buffered saline pH7.4 (PBS) and fixed in 4% paraformaldehyde (PFA in PBS) for 1 h at room temperature (20 °C to 24 °C), whereas human neural stem cells (hNSCs) were fixed in 4% PFA at 4 °C for 10 min. Embryonic mouse brains were cryoprotected (30% sucrose in PBS) before being embedded in gelatin for cryosectioning at 14 μ m (Leica) onto slides (SuperFrost Plus, VWR International). Fluorescent immunohistochemistry was performed as previously described⁴⁰. In summary, antigen retrieval (Dako Target Retrieval Solution) of mouse brains were performed at 95 °C for 15 min before incubation with primary antibodies. The following primary antibodies were used: anti-PDI, anti-calreticulin and anti-calnexin (1:300, rabbit, #92516 ER-stress kit from Cell Signaling Technology); anti-cleaved-caspase-3 (1:100, rabbit, #9661, CST), anti-Tbr1 (1:200, rabbit, ab31940, Abcam), anti-Tbr2 (1:500, rat, 14-4875-82, eBioscience), anti-Ki67 (1:100, mouse, 550609, BD Pharmingen), anti-Sox2 (1:200, goat, sc-17320, Santa Cruz), anti-flavivirus group antigen (1:1,000, mouse, MAB10216, Millipore), anti-NS1 from dengue virus conjugated with Alexa Fluor-546 (1:500, isolated by M.F.¹³), anti-Pax6 (1:500, mouse, AB528427, DSHB), anti-GFP (1:1,000, rabbit, TP401, Torrey Pines Biolabs), anti-GFP (1:1,500, goat, ab6673, Abcam), anti-Sox1 (1:500, goat, AF3369, RD System), anti-nestin (1:500, chicken, NB100-1604, Novus Biologicals), anti-Ctip2 (1:100, rat, ab28448, Abcam), anti-Satb2 (1:2,000, rabbit, ab92446, Abcam) and anti-Tuj1 (1:250, mouse, MMS-435P, Covance). The respective secondary antibodies used were anti-mouse, anti-rabbit, anti-rat, anti-chicken or anti-goat antibodies, conjugated with Alexa Fluor-488, Alexa Fluor-555, Alexa Fluor-405 or Alexa Fluor-647 (Jackson ImmunoResearch Laboratories or Life Technologies) and diluted at 1:800. Nuclei were counterstained with DAPI (1:10,000, Sigma) or Hoechst (1:5,000, Thermo Fisher Scientific) and mounted in Mowiol (Sigma) solution.

Virus production. ZIKV H/PF/2013, yellow fever 17D (YFV) and West Nile NY99 (WNV) were amplified on mosquito C6/36 cells, and supernatants were harvested and frozen at -80 °C. Titer of virus stock was determined by tissue cytopathic infectious dose 50 (TCID₅₀) on Vero cells, and viral titers were expressed as TCID₅₀/mL. Manipulation and in vivo injection of ZIKV, WNV and YFV 17D were authorized by the Animal Ethics Committee of the University of Liège (#16-1829).

Induction of hNSCs from hIPSCs and ZIKV infection. Approvals of the Ethics Committee of the University of Liège for research and protocols (#B70720096309), and patient informed consents were obtained before deriving hIPSCs from skin fibroblasts isolated by punch biopsies. All experiments were conducted according to the guidelines of the Ethics Committee of the University of Liège. The hNSCs were generated from human skin fibroblast reprogrammed hIPSC from healthy donors following the procedure described in ref. ²⁵. The hNSCs (purity of 87.9 \pm 2.4, n = 3 to 6 cultures) were maintained on poly-ornithine/laminin coated dishes and cultured in the neural induction medium: 50–50% DMEM/F12

Neurobasal medium supplemented with 2% B27, 1% N-2, 0.5% Glutamax (35050-038 Gibco), 10 ng/mL epidermal growth factor (EGF; AF-100-15 Peprtech) and 10 ng/mL bFGF. For ZIKV infection of hNSCs (purity of 85.6 \pm 2.0, n = 3 to 6 cultures), cells at early stages were seeded in 6- and 24-well plates with coverslips 24 h before the infection. In all experiments, human neuronal progenitors were seeded in 6- and 24-well plates on coated coverslips at densities of 3 \times 10⁵ and 6 \times 10⁴ respectively, and infected at MOI5 (multiplicity of infection) or treated with mock medium for 2 h. The medium was then replaced with fresh neural induction medium, and the NSCs were fixed in Trizol or 4% PFA, 24 h or 48 h after infection for qRT-PCR or immunofluorescence experiments, respectively.

RNA extraction and qRT-PCR analyses. Total RNA was obtained from microdissected embryonic mouse brains and neuronal progenitors seeded in 6-well culture dishes after application of Trizol, according to the manufacturer's protocol (Ambion-Life Technologies, 15596018).

The quantity and quality of RNA were assessed by NanoDrop 1000 (NanoDrop Technologies) before cDNA synthesis by SuperScript III reverse transcriptase (Invitrogen), according to the manufacturer's instructions. The resulting cDNA was used for quantitative PCR, using Faststart Universal SYBR Green Master (Roche) in an Applied Biosystems 7900HT Fast Real-Time PCR detection system (Applied Biosystems, Foster City, USA). The genes of interest (GOI) in Supplementary Table 1 were normalized to the reference genes: β -actin (*ACTIN*), glyceraldehyde-3-phosphate dehydrogenase (*GAPDH*), hypoxanthine phosphoribosyltransferase 1 (*HPRT1*), and 36b4 ribosomal protein (*36B4*). See Supplementary Table 1.

Intracerebral (ICV), intraplacental (IPL) injections, and in utero electroporation (IUE). Immunocompetent NMRI wild-type adult mice (2–3 months of age) were purchased from Janvier Laboratories, France, and Envigo Laboratories, the Netherlands. Timed-mated pregnant dams were housed in a specific-pathogen-free facility under standard conditions and allowed to acclimate for more than 24 h, with ad libitum access to food and water. The surgeries were performed at the same time of day, when noon of the day after mating was considered E0.5. Preoperative analgesia was administered subcutaneously with Temgesic (buprenorphine 0.1 mg/kg body weight, Schering-Plough, Brussels, Belgium) before induction of anesthesia with isoflurane (Abbot Laboratories Ltd, Kent, UK) in an oxygen carrier. Following this a minilaparotomy was performed with a 1.0- to 1.5-cm incision through the lower ventral peritoneum; the uterine horns were careful extracted onto warm humidified gauze pads. The intracerebroventricular (ICV)³⁹ or intraplacental (IPL)³³ injections of embryos at E12.5 as well as in utero electroporation (IUE)³⁹ of embryos at E13.5 were performed as previously described with slight modifications.

The animals were randomly assigned to receive a 1.0- to 2.0- μ L injection of mock media, Zika (ZIKV H/PF/2013, 1.6 \times 10⁷ TCID₅₀/mL), yellow fever (YFV 17D, 1.6 \times 10⁷ TCID₅₀/mL) or West Nile (WNV NY99, 1.6 \times 10⁷ TCID₅₀/mL) viruses. All procedures with ZIKV and YFV were conducted within a BSL2, whereas those with WNV were conducted within a BSL3 animal containment facility. In utero electroporation was performed with pCAGGS-IRES-GFP (1 μ g/ μ L) or in combination with either *Chop* siRNA (10 μ M) or control siRNA (10 μ M) into the ipsilaterally infected vesicle at E13.5, as indicated. Five electrical pulses were applied at 30 mV (50 ms duration) across the uterine wall of E13.5 pregnant mice at 950-ms intervals using 3-mm platinum tweezers electrodes (CUY650P3, Sonidel, Ireland) and an ECM-830 BTX square-wave electroporator (VWR International). The plasmid DNA was purified using a Plasmid Endofree Maxi Kit (Qiagen, Hilden, Germany) and sequence-verified. The inhibitors of PERK (GSK2656157, 'PERKⁱ', used at 10 μ M or 50 μ M as indicated in figure legends) and IRE-1 (4 μ 8 C, 'IRE-1ⁱ', used at 800 μ M) were concomitantly administered with either ZIKV or mock media at E12.5 and with the pCAGGS-IRES-GFP solution at E13.5 as indicated. All solutions were mixed with 0.05% Fast Green (Sigma, Bornem, Belgium) before injections by a Femtojet microinjector (VWR International) in a pulled borosilicate needle.

Timed-mated IFN- α/β R^{-/-} mice were infected intraperitoneally at E9.5 with 100 μ L of ZIKV (1 \times 10⁷ TCID₅₀/mL). Five days after infection, pregnant mice were killed for analysis at E14.5 by neck dislocation and the cerebral cortex of each fetus was collected.

Neuro2A cell culture. Neuroblastoma Neuro-2A cells were cultured according to conventional protocol (ATCC CCL-131). Silencer Select predesigned and validated siRNAs (ThermoFisher Scientific) were used to suppress expression of *Chop*. The efficacy was evaluated by Mirus (Mirus Bio) transfection of siRNA into neuroblastoma Neuro-2A cells, followed by quantitative real-time polymerase chain reaction (q-RT-PCR) 48 h after transfection, as previously reported⁴⁰.

Quantification of virus copy number in infected tissues and cells. The number of Zika particles in the samples analyzed by qRT-PCR (see above) was calculated as previously described⁴¹. Briefly, a standard curve was created by performing serial dilutions of a plasmid containing a 76-bp long sequence (inserted BamHI/XhoI) from the Zika genome (from nt 1,086 to 1,162) and querying these dilutions by qRT-PCR analysis. The following primers were used to create the standard curve: ZIKV 1,086 (genome pos. 1,086–1,102): 5'-CCGCTGCCCAACACAAG-3';

ZIKV: 1,162c (genome pos. 1,162–1,139): 5'-CCACTAACGTTCTTTGCGACAT-3'. This standard curve allows the conversion of C_p of samples queried for Zika virus (as described above) into N° of Zika copies/ μ L. We used the following formula to link this quantification to the amount of RNA retrotranscribed for the analysis of each sample:

$$\text{Number}(N^\circ) \text{ of copies}/\mu\text{L} \times k \times d \times P = N^\circ \text{ copies}/\mu\text{g RNA}$$

where k is a correction factor introduced to calculate the N° of copies with respect to 1 μ g of RNA (in this instance 0.5 μ g of RNA were used to synthesize cDNA, so $k=2$), d is a dilution factor, taking into account the dilution of cDNA used for the analysis (in this case the cDNA was diluted 1:30, so $d=30$) and P is a correction factor introduced to calculate the N° of Zika copies with respect to the total amount of cDNA (here 3.4 μ L on a total of 20 μ L of cDNA mix were used, so $P=5.88$).

Finally, the N° of copies/ μ g RNA was divided for the relative concentration of each sample analyzed by qRT-PCR (since for each analyzed gene in this study we performed a relative quantification compared to the controls of the same experiment). The relative concentration of each sample is automatically calculated by the LightCycler480 and its accompanying software.

Transmission electron microscopy. Human fetal cortical samples and E14.5 mouse brains were fixed at 4 °C, for 24 and 2 h respectively, in 2.5% glutaraldehyde in 0.1 M Sørensen's buffer (0.2 M NaH_2PO_4 , 0.2 M Na_2HPO_4 , pH 7.4) for 2 h. Human fetal cortical samples were fixed at 4 °C in the same solution for 24 h. After several washes in Sørensen's buffer, the mouse and human samples were postfixed at 4 °C with 2% osmium tetroxide in Sørensen's buffer for 60 min, then washed in deionized water, dehydrated at room temperature through a graded ethanol series (70, 96 and 100%) and embedded in Epon for 48 h at 60 °C. Ultrathin 70-nm sections were obtained by means of an ultramicrotome (Reichert Ultracut E) equipped with a diamond knife (Diatome). The sections were mounted on copper grids coated with collodion and contrasted with uranyl acetate and lead citrate for 15 min each.

Image acquisition and manipulation. For immunofluorescent images of embryonic brain and hNSCs sample, magnified fields (20 \times , 40 \times and 60 \times) were acquired with either the Nikon A1 or the Zeiss LSM 880 AiryScan Elyra S.1 confocal microscopes and further processed with ImageJ 1.42q 276 (Wayne Rasband, National Institutes of Health) and Fiji (version 2.0.0-rc-54/1.51 h, <https://imagej.net/Fiji>) software. Fluorescence levels of Pax6 were divided by corresponding DAPI fluorescence levels, followed by normalization to that of Mock group and expressed as arbitrary units. ZIKV immunofluorescence levels were quantified as ROIs (50 μ m \times 50 μ m) in the cortical wall and divided for corresponding DAPI fluorescence levels. Values were normalized to those of the ZIKV DMSO group and expressed as arbitrary units. The ultrathin transmission electron microscopy sections were observed under a JEM-1400 transmission electron microscope (Jeol) at 80 kV and photographed with an 11 megapixel bottom-mounted TEM camera system (Quemesa, Olympus). The images were analyzed via RADIUS software (Olympus, version 2.0).

Protein extraction and western blot. Proteins for western blot analysis were extracted from E15.5 mouse brains injected at E12.5 with either simple culture medium (mock) or Zika virus. Once collected, the brains were stored in Trizol (Ambion-Life Technologies, 15596018) at -80 °C before use. RNA and proteins were consecutively extracted from the same samples according to the Trizol manufacturer's protocol. Extracted proteins were finally resuspended in a solution of 0.5% SDS/4 M urea and quantified by NanoDrop 1000 (Nano-Drop Technologies). Proteins (20 μ g) were mixed with loading buffer four times (200 mM Tris-Cl pH 6.8, 4% β -mercaptoethanol, 8% SDS, 0.4% bromophenol blue, 40% glycerol), incubated for 5 min at 95 °C, separated by SDS-PAGE and blotted on a nitrocellulose membrane (Hybond ECL, GE Healthcare Life Science). The following antibodies were used to detect UPR factors: rabbit anti-PERK (1/500, #3192, Cell Signaling), rabbit anti-p-PERK (Thr 980; 1/500, #3179, Cell Signaling), rabbit anti-eIF2 α (D7D3) XP (1/500, #5324, Cell Signaling), rabbit anti-phospho-eif2 α

(Ser51; D9G8; XP; 1/500, #3398, Cell Signaling), rabbit anti-IRE1 α (14C10; 1/500, #3294, Cell signaling), anti-phospho-IRE1 α (S724; 1/500, Abcam, ab48187) and Atf6 (1/100, #65880, Cell Signaling). To enhance the detection of specific bands, the membrane was incubated for 10 min in antigen pretreatment solution (Supersignal Western Blot Enhancer kit, Thermo Scientific) and then for 1 h in 3% BSA / TBS Tw 0.1%. Primary antibodies were diluted in primary antibody diluent (Supersignal Western Blot Enhancer kit, Thermo Scientific) and the incubation with the membrane lasted 2 h at RT. Primary antibodies were detected by the use of an HRP-conjugated anti-rabbit antibody (1/10,000, RPN4301, GE Healthcare) and the membranes were developed with Pierce-ECL Western Blotting Substrate (Thermo Scientific). Images of membranes were taken by ImageQuant LAS 4000 (GE Healthcare Life Science; see Supplementary Fig. 6).

Experimental design and randomization. No statistical methods were used to predetermine sample sizes, but our sample sizes are similar to and based on those reported in previous publications of neurogenic balance during cortical development^{15,17,42}. Cultured hNSCs in 6- and 24-well plates were randomly allocated to either the mock or ZIKV infections. All time-mated pregnant dams and embryos were randomly allocated to the different treatments during the surgeries. Each replicate in all animal studies herewithin was considered as one individual mock-treated or viral-infected embryo.

Statistical analysis. Single blinding was performed, whereby information regarding treatment of each sample was not transferred between the animal surgeon, the microscopist and analyst until the final data were acquired for statistical analyses. GraphPad Prism software (version 6.02) was used for the analyses, where statistical tests were applied according to the distribution, variance and normality of each dataset. As specified in the figure legends, all dual comparisons were performed using either unpaired two-tailed Student's t tests for parametric datasets or one- or two-sided Mann-Whitney tests for nonparametric datasets. Additionally, multiple comparisons were performed with one- or two-way ANOVA followed by Bonferroni post hoc tests for parametric datasets and with Kruskal-Wallis followed by Dunn's post hoc tests for nonparametric datasets, as specified in the figure legends. Levels of significance: **** $P < 0.0001$, *** $P < 0.001$, ** $P < 0.01$, * $P < 0.05$ for all statistics herein; and ns means not significant. The number of biological replicates in each experiment is specified in the figure legends. No samples were excluded from analyses.

Life Sciences Reporting Summary. Further information on experimental design is available in the Life Sciences Reporting Summary.

Data availability. The authors declare that all data supporting the findings are available from the corresponding authors upon reasonable request.

References

- Lambert, N. et al. Genes expressed in specific areas of the human fetal cerebral cortex display distinct patterns of evolution. *PLoS One* **6**, e17753 (2011).
- Cau, E., Gradwohl, G., Fode, C. & Guillemot, F. Mash1 activates a cascade of bHLH regulators in olfactory neuron progenitors. *Development* **124**, 1611–1621 (1997).
- Gladwyn-Ng, I. E. et al. Bacurd2 is a novel interacting partner to Rnd2 which controls radial migration within the developing mammalian cerebral cortex. *Neural Dev.* **10**, 9 (2015).
- Gladwyn-Ng, I. E. et al. Bacurd1/Kctd13 and Bacurd2/Tnfrsf1 are interacting partners to Rnd proteins which influence the long-term positioning and dendritic maturation of cerebral cortical neurons. *Neural Dev.* **11**, 7 (2016).
- Lanciotti, R. S. et al. Genetic and serologic properties of Zika virus associated with an epidemic, Yap State, Micronesia, 2007. *Emerg. Infect. Dis.* **14**, 1232–1239 (2008).
- Tielens, S. et al. Elongator controls cortical interneuron migration by regulating actomyosin dynamics. *Cell Res.* **26**, 1131–1148 (2016).

Life Sciences Reporting Summary

Nature Research wishes to improve the reproducibility of the work that we publish. This form is intended for publication with all accepted life science papers and provides structure for consistency and transparency in reporting. Every life science submission will use this form; some list items might not apply to an individual manuscript, but all fields must be completed for clarity.

For further information on the points included in this form, see [Reporting Life Sciences Research](#). For further information on Nature Research policies, including our [data availability policy](#), see [Authors & Referees](#) and the [Editorial Policy Checklist](#).

▶ Experimental design

1. Sample size

Describe how sample size was determined.

The sample sizes were based on previous studies of neurogenic balance during cortical development. (See Main text > Material and Methods > Experimental Design and Randomization).

2. Data exclusions

Describe any data exclusions.

No data was excluded.

3. Replication

Describe whether the experimental findings were reliably reproduced.

All data from post-optimized replications were included in the statistical analysis. (See Supplementary Information > Material and Methods > Experimental Design, and Supplementary Information > Material and Methods > Cell Counting and Statistical Analysis).

4. Randomization

Describe how samples/organisms/participants were allocated into experimental groups.

All time-mated pregnant dams and embryos were randomly allocated to the different treatments during the surgeries. Cultured hNSCs in 6- and 24- well plates were randomly allocated to either the Mock or ZIKV infection. (See Supplementary Information > Material and Methods > Experimental Design)

5. Blinding

Describe whether the investigators were blinded to group allocation during data collection and/or analysis.

Single blinding was performed, whereby information regarding treatment of each sample was not transferred between the animal surgeon, the microscopist and analyst, until the final data was acquired for statistical analyses.

Note: all studies involving animals and/or human research participants must disclose whether blinding and randomization were used.

6. Statistical parameters

For all figures and tables that use statistical methods, confirm that the following items are present in relevant figure legends (or in the Methods section if additional space is needed).

n/a Confirmed

- The exact sample size (n) for each experimental group/condition, given as a discrete number and unit of measurement (animals, litters, cultures, etc.)
- A description of how samples were collected, noting whether measurements were taken from distinct samples or whether the same sample was measured repeatedly
- A statement indicating how many times each experiment was replicated
- The statistical test(s) used and whether they are one- or two-sided (note: only common tests should be described solely by name; more complex techniques should be described in the Methods section)
- A description of any assumptions or corrections, such as an adjustment for multiple comparisons
- The test results (e.g. P values) given as exact values whenever possible and with confidence intervals noted
- A clear description of statistics including central tendency (e.g. median, mean) and variation (e.g. standard deviation, interquartile range)
- Clearly defined error bars

See the web collection on [statistics for biologists](#) for further resources and guidance.

► Software

Policy information about [availability of computer code](#)

7. Software

Describe the software used to analyze the data in this study.

The statistical softwares used was GraphPad Prism software (version 6.02). The imaging software used were ImageJ (version 1.42q 276), FIJI (version 2.0.0-rc-54/1.51h), and RADIUS (Olympus, version 2.0) (See Main Text > Material and Methods > Statistical Analysis, Main Text > Material and Methods > Image acquisition and manipulation, Main Text > Material and Methods > Transmission Electron Microscopy).

For manuscripts utilizing custom algorithms or software that are central to the paper but not yet described in the published literature, software must be made available to editors and reviewers upon request. We strongly encourage code deposition in a community repository (e.g. GitHub). *Nature Methods* [guidance for providing algorithms and software for publication](#) provides further information on this topic.

► Materials and reagents

Policy information about [availability of materials](#)

8. Materials availability

Indicate whether there are restrictions on availability of unique materials or if these materials are only available for distribution by a for-profit company.

There are neither restrictions on availability of unique materials, nor for distribution by a for-profit company.

9. Antibodies

Describe the antibodies used and how they were validated for use in the system under study (i.e. assay and species).

The manufacturers, catalog numbers, and specific concentrations of all pre-validated primary and secondary antibodies used were stated in the Main Text > Material and Methods > Immunohistochemistry, and Main Text > Material and Methods > Protein extraction and Western blot. For immunohistochemistry, the following primary antibodies were used: anti-PDI, anti-Calreticulin and anti-Calnexin (1:300, rabbit, #92516 ER-stress kit from CST (Cell Signaling Technology)); anti-Cleaved Caspase 3 (1:100, rabbit, #9661, CST), anti-Tbr1 (1:200, rabbit, ab31940, Abcam), anti-Tbr2 (1:500, rat, 14-4875-82, Ebioscience), anti-Ki67 (1:100, mouse, 550609, BD Pharmingen), anti-Sox2 (1:200, goat, sc-17320, Santa Cruz), anti-Flavivirus Group Antigen (1:1000, mouse, MAB10216, Millipore), anti-NS1 from Dengue Virus conjugated with Alexa-546 (1:500, isolated by Marie Flamand) anti-Pax6 (1:500, mouse, AB528427, DSHB), anti-GFP (1:1000, Rabbit, TP401, Torrey Pines Biolabs), anti-GFP (1:1500, Goat, ab6673, Abcam), Anti-Sox1 (1:500, Goat, AF3369 RD System), anti-Nestin (1:500, chicken, NB100-1604, Novus Biologicals), anti-Ctip2 (1:100, rat, ab28448, Abcam), anti-Satb2 (1:2000, rabbit, ab92446, Abcam), anti-Tuj1 (1:250, mouse, MMS-435P, Covance). The respective secondary antibodies used were (1:800; anti-mouse, anti-rabbit, anti-rat, anti-chicken or anti-goat) conjugated either with Alexa-488, Alexa-555, Alexa 405 or Alexa-647 (Jackson ImmunoResearch Laboratories or Life Technologies). The validation of the anti-NS1 antibody from Dengue Virus conjugated with Alexa-546 was performed in ZIKV-infected embryonic mouse brains and compared with commercially available anti-ZIKV antibody (Milipore MAB10216 clone 4G2) as shown in Supplementary Figures S3A and S3B. For immunoblotting, the following antibodies were used to detect UPR factors: rabbit anti-PERK (1/500, #3192, Cell Signalling), rabbit anti-p-PERK (Thr 980) (1/500, #3179, Cell Signalling), Rabbit anti-eIF2 α (D7D3) XP[®] (1/500, #5324, Cell Signalling), Rabbit anti-phospho-eif2 α (Ser51) (D9G8) XP[®] (1/500, #3398, Cell Signalling), rabbit anti-IRE1 α (14C10) (1/500, #3294, Cell signalling), anti-phospho-IRE1 α (S724) (1/500, Abcam, ab48187), Atf6 (1/100, #65880, Cell Signalling).

10. Eukaryotic cell lines

a. State the source of each eukaryotic cell line used.

The only eukaryotic cell line used was human neural stem cells derived from generated from human skin fibroblast reprogrammed hiPSC from healthy donors following the procedure described in Borgs et al doi:10.1038/srep33377 (2016). (See Supplementary Information > Material and Methods > Induction of hNSCs from hiPSCs and ZIKV infection).

b. Describe the method of cell line authentication used.

The human neural stem cells were authenticated through qRT-PCR and immunohistochemistry analyses of expression of human neural stem cell markers.

c. Report whether the cell lines were tested for mycoplasma contamination.

The cell line tested negative for mycoplasma contamination.

d. If any of the cell lines used are listed in the database of commonly misidentified cell lines maintained by [ICLAC](#), provide a scientific rationale for their use.

No common misidentified cell lines were used.

► Animals and human research participants

Policy information about [studies involving animals](#); when reporting animal research, follow the [ARRIVE guidelines](#)

11. Description of research animals

Provide details on animals and/or animal-derived materials used in the study.

Time-mated immunocompetent NMRI (Janvier Labs, Saint Berthevin, France) were operated on either embryonic day E12.5 to E14.5. Time-mated IFN- α /BR-/- mice were operated on at embryonic day E9.5 (See Supplementary Information > Material and Methods > Animals, and Supplementary Information > Material and Methods > Intracerebroventricular (ICV) and intraperitoneal (IPL) ZIKV injection, and in utero electroporation).

12. Description of human research participants

Describe the covariate-relevant population characteristics of the human research participants.

Human fetal brain material were obtained following medical pregnancy termination and processed as described in Lambert et al doi:10.1371/journal.pone.0017753 (2011). (also see Supplementary Information > Material and Methods > Human fetal cortical samples).